Equilibrium shapes and surface selection of nanostructures in 6H-SiC

Sosuke Kondo[a,*], Chad M. Parish[b], Takaaki Koyanagi[b], Yutai Katoh[b]

[a] Institute of Advanced Energy, Kyoto University, Uji, Kyoto 611-0011, Japan.
[b] Oak Ridge National Laboratory, Oak Ridge, Tennessee 37831, USA

*Corresponding author.
E-mail addresses: kondo@iae.kyoto-u.ac.jp (S. Kondo)

Abstract

The equilibrium shape of 6H-SiC nanostructures and their surfaces were studied by analyzing nano-void (~10 nm) shapes, which were introduced in monocrystalline 6H-SiC by high-temperature neutron irradiation, using transmission electron microscopy. The nano-voids were determined to be irregular icosahedrons truncated with six $\{\bar{1}100\}$, twelve $\{\bar{1}103\}$, one smaller top-basal, and one larger bottom-basal planes, which suggests that $\{\bar{1}100\}$ and $\{\bar{1}103\}$ are the next stable surface class after the basal planes. The relatively frequent absence of the $\{\bar{1}100\}$ surface in the nano-voids indicated that the $(\bar{1}10\bar{3})$ surface type is energetically rather stable. These non-basal surfaces were found not to be atomically flat due to the creation of nanofacets with half unit-cell height in the c-axis. The $\{\bar{1}100\}$ and $\{\bar{1}103\}$ surfaces were classified as two and four face types according to their possible nanofacets and surface termination, respectively. We also discuss the surface energy difference between the $(\bar{1}10\bar{3})$ and $(\bar{1}103)$ face types in relation to the energy balance within the equilibrium, but irregular, polyhedron, in which the $(\bar{1}103)$ surface had double the surface energy of the $(\bar{1}10\bar{3})$ surface (~3900 erg/cm^2).

Silicon carbide (SiC) nanostructures have attracted much interest from the materials and device communities because of their unique properties that make them well suited for applications in microelectronics and optoelectronics [1-3]. The efficiency and the band-shift of visible light emissions from these nanostructures depend on their shape and size [4,5]. The theoretical studies on the structure and electronic properties of SiC nanostructures predict that the band gap of nanostructures strongly depends on their size and/or dangling-bond surface states [6-8]. Therefore, synthesis of such nanostructures in a variety of morphologies, including nanoboxes, hollow nanospheres, nanorods, and nanowires, have been studied to reveal their quantum confinement effects and enable full control of the spontaneous formation of SiC nanostructures [9-12]. For efficient synthesis and formation of stable nanostructures, the growth morphologies should not deviate far from the equilibrium shapes. The equilibrium shape, or Wulff shape, of a crystal grown under thermodynamic equilibrium results from minimization of the total surface energy in a given volume. The most common and technologically advanced SiC polytypes are 2H-, 4H-, and 6H-SiC with hexagonal symmetries, as well as 3C-SiC with a cubic structure. The equilibrium shape of cubic SiC has been reported to be a tetrahedron or octahedron faceted with {111} lattice planes as a consequence of their lowest surface energy [13,14]. However, non-cubic systems with intermediate hexagonality, such as 4H- (50% hexagonal stacking) and 6H-SiC (33.3% hexagonal stacking), complicate the Wulff construction and even the surface energy due to the mixture of cubic and hexagonal stacking of Si-C bi-layer. Although the basal planes are known to be the most stable surfaces for hexagonal SiC, the surface stability of other surfaces is still unclear despite its importance for atomic control during epitaxial growth. The shape of “macroscopic” growth nuclei or etch pits on 6H-SiC basal planes are also often found to be hexagonal with flat basal top (or bottom) and $\{01\bar{1}0\}$ side walls [15,16]. However, kinetics and/or kink “gateway for migrating atoms” density, in addition to energetics, play an important role in determining such a macroscopic crystalline shape. The importance of the surface energy increases as the volume of the structure decreases, increasing the surface-to-volume ratio. Therefore, sufficiently small internal voids or spontaneous aggregates of vacancies that are isolated from the external environment would be beneficial for determining the equilibrium of a nanostructure. Such voids have been observed in many materials that were irradiated with neutrons [13,17-19], since collisions between neutrons and lattice atoms produce supersaturated migrating vacancies. In this study, the three-dimensional structure of the polyhedral voids formed in 6H-SiC

during high-temperature neutron irradiation was addressed using transmission electron microscopy (TEM) to reveal stable atomic surfaces other than basal planes.

Single-crystal 6H-SiC samples produced by Cree Research Inc. were irradiated with neutrons at a fluence of 6×10^{25} n/m^2 (> 0.1 MeV) at 1460 ± 100 °C in an ultrahigh-purity inert gas environment in the High Flux Isotope Reactor at the Oak Ridge National Laboratory. Due to the lower atomic mass and displacement threshold energy of the C atoms on the C sublattice, relative to those of the Si atoms on the Si sublattice, about three to four times more C atoms than Si atoms were displaced. Two thin foils, <0001> and $<01\bar{1}0>$ foil normal, were prepared in a commercial focused ion-beam unit (FEI Versa3D) with 5- to 30-keV Ga-ions, followed by surface treatment with 600-eV Ar-ions (Fishione Nanomill). The thin foils were examined using a field-emission TEM (FE-TEM/FEI Talos F200X, 200 keV).

Typical microstructures of 6H-SiC irradiated with neutrons at 1460 °C are shown in Fig. 1a-c. The relationship between a 6H structure of unit height and the respective viewing directions in Fig. 1a-c are indicated in Fig. 1d, in which each blue and yellow atom represents either a Si or a C atom. The unit cell consists of six Si-C bilayers stacked in the order ABCACB, as labeled, where the Si-C bond directions rotate 60° about the c axis between the ABC and ACB bilayers. A number of polygonal defects, typically ~10 nm in size, which were confirmed not to be present in non-irradiated specimens, can be seen in Fig. 1a-c. Through-focus and high-angle annular dark-field imaging revealed that the polygonal defects are voids without any stacking faults or dislocations. The number density of voids was estimated to be 3×10^{22} m^{-3}, similar to that of the tetrahedral voids in 3C-SiC irradiated under similar irradiation conditions [19]. Trapezoidal dislocation loops, which are essentially two-dimensional aggregates of interstitials on the basal plane [20,21], are also observed in Fig. 1a, as indicated by the arrow. The dense lines formed on the basal planes in Fig. 1b and c are loops. The magnified plane-view images of typical polygonal voids, captured from three different directions, namely, [0001], $[11\bar{2}0]$, and $[01\bar{1}0]$, are also shown in Fig. 1a-c, respectively. Most voids viewed from [0001] appeared as regular hexagons, with each side perpendicular to the <01-11> direction. Side views of these regular hexagonal defects using B = $[11\bar{2}0]$ and $[01\bar{1}0]$ show that the top and bottom surfaces of the voids are faceted by two basal planes, as shown in Fig. 1b and c, respectively. The typical shapes, viewed both from $[11\bar{2}0]$ and $[01\bar{1}0]$, are very similar, and are mostly polygonal, having eight vertices and eight sides. The relatively

shorter sides perpendicular to <$\bar{2}$110> or <$\bar{2}$116>, however, are often somewhat rounded, as shown in Fig. 1c.

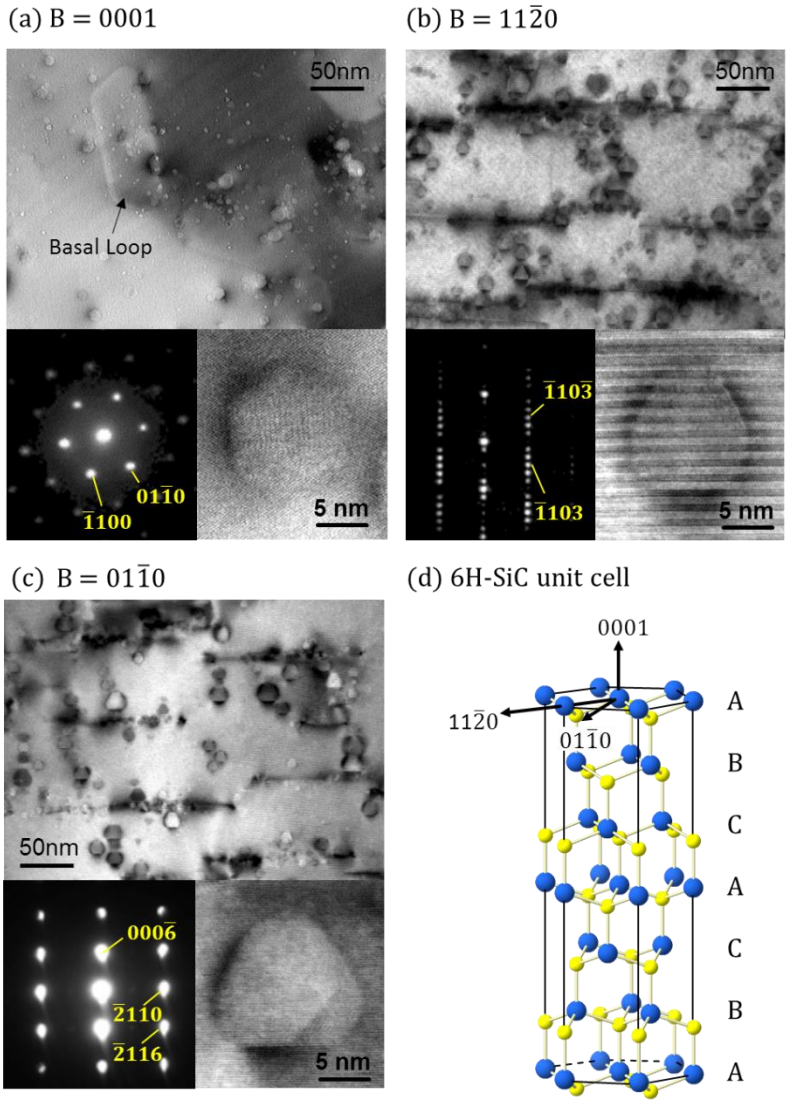

FIG. 1 Transmission electron microscope images of 6H-SiC irradiated with neutrons at 1460 °C. Voids are viewed from three different directions, namely, (a) [0001], (b) [$11\bar{2}0$], and (c) [$01\bar{1}0$]. The image (a) was taken from a basal foil. The images (b, c) were taken from almost the same location in the thin foil with foil normal near [$01\bar{1}0$]. The viewing directions are schematically illustrated in (d).

Figure 2 is a typical void image as viewed from [$11\bar{2}0$]. Note that the length of the basal bottom side is always larger than that of the basal top side in a void,

regardless of whether it is viewed from the [11$\bar{2}$0] or [01$\bar{1}$0] direction. In response to this, the length of the side perpendicular to <$\bar{1}$10$\bar{3}$> is always larger than that of the side perpendicular to <$\bar{1}$103>. The lengths of these sides, inclined relative to the basal plane, appear to be equal to the integral multiple of the unit <$\bar{1}$103> length in most voids. That is, the upper side perpendicular to [$\bar{1}$10$\bar{3}$] contains four ABCACB stacking units, labeled 1a–4a in the figure, while the side perpendicular to [$\bar{1}$103] contains only two stacking units, labeled 1b and 2b. Similarly, most sides perpendicular to [$\bar{1}$100] appear to have lengths that are an integral multiple of the unit cell height on the 6H-SiC(0001) surface. The discrete void height for a step of unit cell height is likely possible due to the surface energy difference between the (000n) (n = 1–6, called 6H1–6, respectively [22,23]). The shorter edge seems to bow slightly towards the outside of the void, likely attributable to localized forces at the edge resulting from discontinuity of the surface stress. Other minority shapes, viewed from B = [11$\bar{2}$0] and [01$\bar{1}$0], are hexagonal and trapezoidal, although the enlarged images are not shown here. The sides perpendicular to <$\bar{1}$100> are missing for the hexagonal shapes, while the sides perpendicular to <$\bar{1}$103> are missing for the trapezoidal ones. These variations are likely due to the energy barrier for adding new facets with associating edges and vertices, and thus the minority shapes are less thermally stable than the majority shapes.

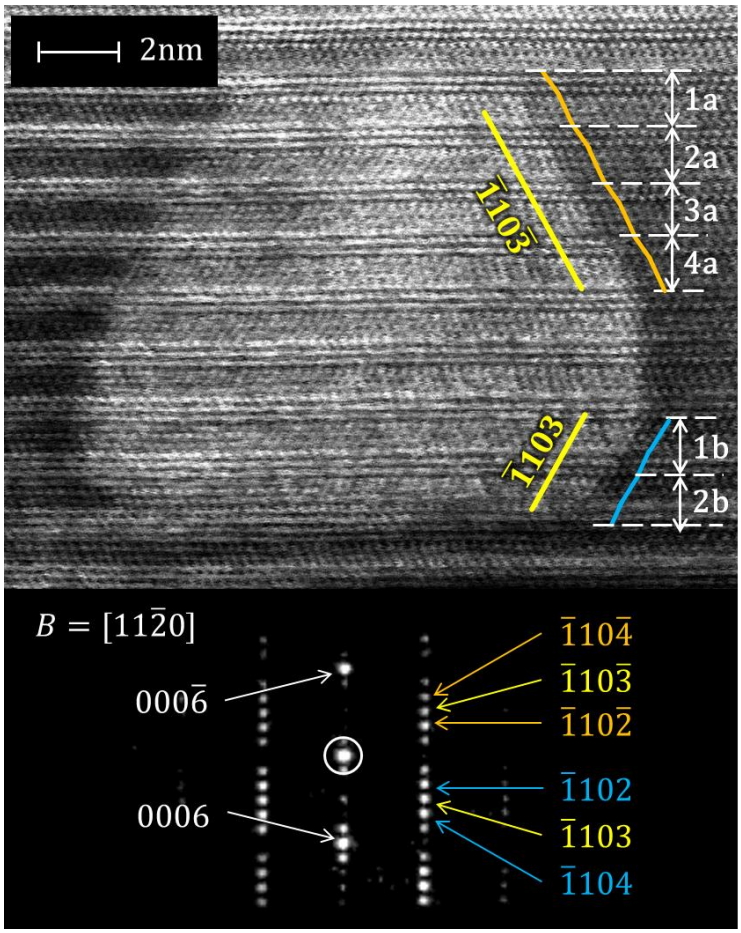

FIG. 2 High-resolution image of a faceted void viewed from the $[11\bar{2}0]$ direction. Each arrow indicates the height of a unit cell containing six Si-C bi-layers, where the height of the upper half region is identical to the height of 4 unit cells and that of the lower half region is identical to that of 2 unit cells. Zigzag lines indicate the void surfaces with nanofacets (see the corresponding surfaces in the same color in Fig. 3).

The most likely three-dimensional void shape, which is consistent with all the views from three different directions (Fig. 1a-c), is schematically illustrated in Fig. 3a, in which the surfaces are color-coded according to the surface type, as discussed later. The shape is an icosahedron truncated with two basal, twelve $\{\bar{1}103\}$, and six $\{\bar{1}100\}$ planes. This indicates that all eight sides observed from a viewing direction of $[11\bar{2}0]$ (Figs. 1b and 2) are edge-on void surfaces. The twelve $\{\bar{1}103\}$ surfaces would be divided into two groups belonging to either the upper or

lower half of the void, and both groups are further classified geometrically into two types, as discussed below. In contrast to the regular icosahedron that would be expected in a cubic crystal, with twenty geometrically equal {111} facets, 12 corners, and 30 edges, the icosahedral facets in 6H-SiC have a six-fold symmetry about the 0001 rotation axis. The selection of $\{\bar{1}103\}$ surfaces was unexpected, since they have not previously been observed for either the etch pits or crystalline domains of epitaxial nuclei, despite their six-fold shapes with 0001 rotation axes and frequent $\{\bar{1}100\}$ side walls [24,25].

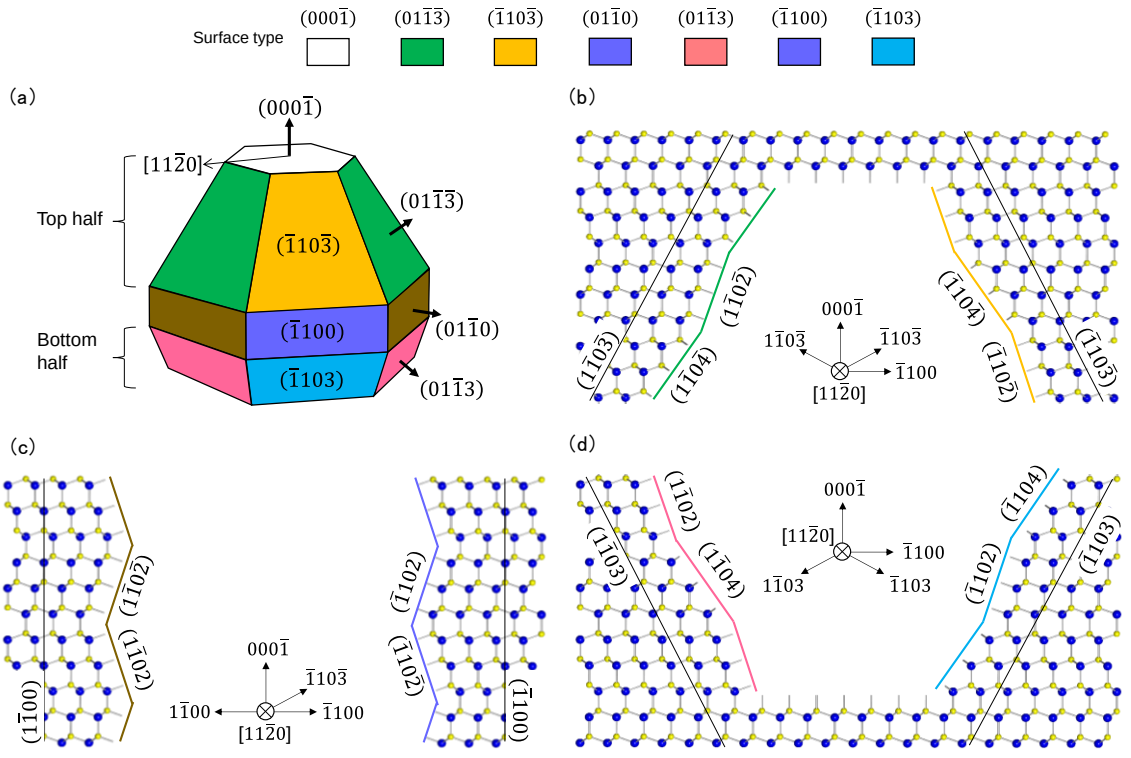

FIG. 3 (a) Schematic illustration of possible three-dimensional void shape, consistent with the plane views from three different directions (see Fig. 1a-c). (b-d) Possible atomic arrangements of the void surfaces with nanofacets, as viewed from three different directions. Such a zigzag surface pattern was also evident in the high-resolution void image (Fig. 2).

Figures 3b and c show one of the possible "un-relaxed" atomic arrangements of the void surfaces of the non-polar $\{\bar{1}100\}$ and semipolar $\{\bar{1}10\bar{3}\}$ families in line with the results shown in Fig. 2, respectively. An atomic

reconstruction, which is generally found on a material surface when exposed to the external environment, is not considered here given the intended goal of this study. All the "hypothetical" void surfaces, except for the basal ones, are not allowed to be atomically flat, as can clearly be seen in Fig. 3b-d. The zigzag surface patterns were also evident in the high-resolution void image as indicated by colored lines for $(\bar{1}10\bar{3})$ and $(\bar{1}103)$ surfaces, respectively, in Fig. 2. It is possible that the surfaces are composed of nanofacets with half unit-cell heights as shown in the figures. For example, the $(\bar{1}10\bar{3})$ surface connects the $(\bar{1}10\bar{2})$ and $(\bar{1}10\bar{4})$ nanofacets (Fig. 3b), while the $(\bar{1}100)$ surface connects the $(\bar{1}102)$ and $(\bar{1}10\bar{2})$ nanofacets (Fig. 3c). Of particular note is the geometrical asymmetry of the two facing void surfaces, such as $(1\bar{1}0\bar{3})|(\bar{1}10\bar{3})$ in Fig. 3b, $(1\bar{1}00)|(\bar{1}100)$ in Fig. 3c, and $(1\bar{1}03)|(\bar{1}103)$ in Fig. 3d, due to the anisotropy of the Si-C bi-layer stacking orientation. That is, for example, the order of the nanofacets for $(1\bar{1}0\bar{3})$ "top-basal$|(1\bar{1}0\bar{4})/(1\bar{1}0\bar{2})/(1\bar{1}0\bar{4})\cdots$" differs from that for $(\bar{1}10\bar{3})$ "top-basal$|(\bar{1}10\bar{2})/(\bar{1}10\bar{4})/(\bar{1}10\bar{2})\cdots$". The same difference in the order of the nanofacets is also found between the vicinal surfaces around the c-axis, as indicated by the individual colors in Fig. 3a, where each surface type is indicated by the corresponding color used in Fig. 3c-d. This means that the equilibrium nanostructure of 6H-SiC does not have rotational symmetry through 30° in the atomic scale, although most of the voids appear symmetrical with respect to the c axis at a lower magnification, as observed in Fig. 1b. The selection of $\{\bar{1}103\}$ with the half-unit nanofacets seems to be energetically reasonable, because of the low edge energy at the nanofacet connection with the low vicinal angle in comparison with the other $\{\bar{1}10n\}$ surfaces [26]. In conclusion, the irregular icosahedron contains six types of faces in addition to the basal ones, as illustrated in Fig. 3a. Observation of the hexagonal shape in the $[11\bar{2}0]$ viewing direction, however, reveals the frequent absence of the $\{\bar{1}100\}$ surfaces from the typical void shape, despite the larger surface to volume ratio without these surfaces. This is likely to be acceptable when the semi-polar $\{\bar{1}103\}$ surface energy is somewhat lower than the non-polar $\{\bar{1}100\}$ surface energy. The $\{11\bar{2}n\}$ (n = 16–21) facet, which is often found at 6H-SiC surfaces after gas etching [26], was not found in the nanostructures studied here.

Unfortunately, the surface termination could not be determined because the surface polarity of the specimen used in this study was unclear. However, the top basal surface of a void should be terminated by the species opposite to that of the

bottom surface, because cleavage at the glide plane, having the highest dangling bond density, is known to be unlikely [27]. Pearson et al. calculated the surface free energies of SiC using many-body potential energy functions, and showed that the C face has a much lower surface free energy level (300 erg/cm^2) than the Si face (2220 erg/cm^2), i.e., $\gamma^t_{basl}/\gamma^b_{basl}$ = 7.4 [28]. In our work, the ratio of the upper and bottom basal void surface areas is estimated to be $S^t_{basl}/S^b_{basl} = 0.25$, suggesting that the larger bottom basal surface leaves the internal $(000\bar{1})$ C faces. If the ratio were to be determined only by the surface energy ratio between the two, we would expect to obtain $\gamma^t_{basl}/\gamma^b_{basl}$ = 4 for the surface energy ratio between the Si and C faces. This seems to be in good agreement with the results by Pearson et al. However, the surface energy difference between $\{\bar{1}10\bar{3}\}$ belonging to the top half of the void and $\{\bar{1}103\}$ belonging to the bottom half, which is expected from the difference in face type, should contribute to the unique equilibrium shape of the voids. The presence of $\{\bar{1}100\}$ seems not to affect the S^t_{basl}/S^b_{basl} ratio because they are parallel to the 0001 axis. We hypothesize that two types of upper $\{\bar{1}10\bar{3}\}$ planes, e.g., $(\bar{1}10\bar{3})$ and $(01\bar{1}\bar{3})$, and two types of lower $\{\bar{1}103\}$ planes, e.g., $(\bar{1}103)$ and $(01\bar{1}3)$, possibly each have the same surface energy, despite the atomic-scale nanofacet asymmetry. Otherwise, most voids do not appear as a regular hexagon in B = [0001] and are not symmetrical with respect to the c axis in B = $[11\bar{2}0]$ and $[01\bar{1}0]$ in conventional TEM images. In turn, the sum of surface tension components between the upper and lower void surfaces should be balanced in the axial direction to achieve an asymmetric shape, as follows:

$$6S^t_{\bar{1}10\bar{3}}\gamma^t_{\bar{1}10\bar{3}}\sin\theta + S^t_{basl}\gamma^t_{basl} = 6S^b_{\bar{1}103}\gamma^b_{\bar{1}103}\sin\theta + S^b_{basl}\gamma^b_{basl} \qquad (1)$$

, where θ is the angle between the surface normal and $[\bar{1}100]$ and superscripts (t and b) denote whether the surface is at the top or bottom of the void. The average surface area ratio of $S^t_{\bar{1}10\bar{3}}: S^t_{basl}: S^b_{\bar{1}103}: S^b_{basl}$ was experimentally estimated to be 0.36:0.25:0.18:1. Thus, a surface energy ratio of $\gamma^b_{\bar{1}103}/\gamma^t_{\bar{1}10\bar{3}} \sim 2$ is suggested between the two semi-polar faces of $\{\bar{1}10\bar{3}\}$ and $\{\bar{1}103\}$ from eq. (1) when we employ Pearson's results for the surface energies of basal surfaces. This is consistent with the idea that the smaller surface energies of the upper $\{\bar{1}10\bar{3}\}$ planes compensate for the excess surface energy of the upper half of the void, estimated from the higher S^t_{basl}/S^b_{basl} ratio compared to the theoretical ratio. Indeed, the lower $\{\bar{1}103\}$ surfaces are missing from the minor trapezoidal voids due to the higher surface energy; the surface area ratio was estimated to be 0.23:0.07:0:1,

which implies that $\gamma^{t}_{\bar{1}10\bar{3}}$ does not significantly deviate from the value of 3900 erg/cm^2, thus $\gamma^{b}_{\bar{1}103}$ is ~7800 erg/cm^2. The surface energy difference between $\{\bar{1}10\bar{3}\}$ and $\{\bar{1}103\}$ is possibly dependent on whether the face is Si-rich or C-rich, although this energy difference is significantly smaller than that of basal surfaces.

In summary, the equilibrium shape of nano-sized voids (~10 nm) in 6H-SiC irradiated with neutrons at 1460 °C was investigated using a TEM. The three-dimensional shape was concluded to be a "six-fold and irregular icosahedron" that was truncated with two hexagon-shaped {0001}, six $\{\bar{1}100\}$, and twelve $\{\bar{1}103\}$ surfaces. Non-basal surfaces can be classified into two or four face types according to their atomic arrangements. The selection of $\{\bar{1}103\}$ was unexpected as they had not previously been reported in growth nuclei or etch pits. By considering the surface energy balance in axial direction, it could be experimentally determined that the $\{\bar{1}10\bar{3}\}$ surfaces belonging to the upper region of the voids have approximately half the surface energy of that of the $\{\bar{1}103\}$ surfaces belonging to the lower region of the nano-sized voids.

Acknowledgements

This work was partially supported by the Office of Fusion Energy Sciences, U.S. Department of Energy, under contract DE-AC05-00OR22725 with UT-Battelle, LLC. A portion of this research used resources at the High Flux Isotope Reactor, a DOE Office of Science User Facility operated by the Oak Ridge National Laboratory. This research was performed using instrumentation (FEI Talos F200X S/TEM) provided by the Department of Energy, Office of Nuclear Energy, Fuel Cycle R&D Program and the Nuclear Science User Facilities.

References

[1] H. Dai, E.W. Wong, Y.Z. Lu, S. Fan, and C.M. Lieber, Nature **375**, 769 (1995).

[2] J.Y. Fan, X.L. Wu, and P.K. Chu, Progress in Materials Science **51**, 983 (2006).

[3] S. Castelletto, B.C. Johnson, V. Ivády, N. Stavrias, T. Umeda, A. Gali, and T. Ohshima, Nature Materials **13**, 151 (2014).

[4] T. Matsumoto, J. Takahashi, T. Tamaki, T. Futagi, H. Mimura, and Y. Kanemitsu, Appl. Phys. Lett, **64**, 226 (1994).

[5] J. Botsoa, J. M. Bluet, V. Lysenko, O. Marty, D. Barbier, and G. Guillot, J. Appl. Phys. **102**, 083526 (2007).

[6] D.H. Feng, Z.Z. Xu, T.Q. Jia, X.X. Li, and S.Q. Gong, Phys. Rev. B **68**, 035334 (2003).

[7] F.A. Reboredo, L. Pizzagalli, and G. Galli, Nano Lett. **4** 801 (2004).

[8] R. Rurali, Phys. Rev. B **71**, 205405 (2005).

[9] C.H. Wang, Y.H. Chang, M.Y. Yen, C.W. Peng, C.Y. Lee, and H.T. Chiu, Adv. Mater. **17**, 419 (2005).

[10] H. Ye, N. Titchenal, Y. Gogotsi, and F. Ko, Adv. Mater. **17**, 1531 (2005).

[11] G. Shen, Y. Bando, and D. Golberg, Crystal Growth & Design **7**, 35 (2007).

[12] G. Wei, W. Qin, G. Wang, J. Sun, J. Lin, R. Kim, D. Zhang, and K. Zheng, J. Phys. D: Appl. Phys. **41**, 235102 (2008).

[13] S. Kondo, Y. Katoh, and L.L. Snead, Appl. Phys. Lett. **93**, 163110 (2008).

[14] H.W. Shim, Y. Zhang, and H. Huang, J. Appl. Phys. **104**, 063511 (2008).

[15] T. Kimoto and H. Matsunami, J. Appl. Phys. **76**, 7322 (1994).

[16] V. Heine, C. Cheng, and R.J. Needs, J. Am. Ceram. Soc. **74**, 2630 (1991).

[17] C. Cawthorne and E.J. Fulton, Nature **216**, 575 (1967).

[18] P.J. Maziasz, J. Nucl. Mater. **205**, 118 (1993).

[19] S. Kondo, Y. Katoh, and L.L. Snead, J. Nucl. Mater. **382**, 160 (2008).

[20] O.I. Lebedev, G.V. Tendeloo, A.A. Suvorova, I.O. Usov, and A.V. Suvorov, J. Elec. Microscopy **46,** (4) 271 (1997).

[21] T. Yano and T. Iseki, Phil. Mag. A **62**, 421 (1990).

[22] T. Kimoto, A. Itoh, H. Matsunami, and T. Okano, J. Appl. Phys. **81**, 3494 (1997).

[23] A. Nakajima, H. Yokoya, Y. Furukawa, and H. Yonezu, J. App. Phys. **97**, 104919 (2005).

[24] J. Takahashi, M. Kanaya, and Y. Fujiwara, J. Cryst. Growth **135**, 61 (1994).

[25] S. Nishino, H. Matsunami, and T. Tanaka, J. Cryst. Growth **45**, 144 (1978).

[26] H. Nakagawa, S. Tanaka, and I. Suemune, Phys. Rev. Lett. **91**, 226107 (2003).

[27] M. Tang and S. Yip, J. Appl. Phys. **76**, 2719 (1994).

[28] E. Pearson, T. Takai, T. Halicioglu, and W.A. Tiller, J. Cryst. Growth **70**, 33 (1984).

Figure Captions

FIG. 1 Transmission electron microscope images of 6H-SiC irradiated with neutrons at 1460 °C. Voids are viewed from three different directions, namely, (a) [0001], (b) $[11\bar{2}0]$, and (c) $[01\bar{1}0]$. The image (a) was taken from a basal foil. The images (b, c) were taken from almost the same location in the thin foil with foil normal near $[01\bar{1}0]$. The viewing directions are schematically illustrated in (d).

FIG. 2 High-resolution image of a faceted void viewed from the $[11\bar{2}0]$ direction. Each arrow indicates the height of a unit cell containing six Si-C bi-layers, where the height of the upper half region is identical to the height of 4 unit cells and that of the lower half region is identical to that of 2 unit cells. Zigzag lines indicate the void surfaces with nanofacets (see the corresponding surfaces in the same color in Fig. 3).

FIG. 3 (a) Schematic illustration of possible three-dimensional void shape, consistent with the plane views from three different directions (see Fig. 1a-c). (b-d) Possible atomic arrangements of the void surfaces with nanofacets, as viewed from three different directions. A zigzag surface pattern was also evident in the high-resolution void image (Fig. 2).